Available online at www.sciencedirect.com
ScienceDirect
Physics Procedia 3 (2010) 1607–1613
Physics Procedia
www.elsevier.com/locate/procedia

Proceedings of HBSM 2009

Single molecule and single quantum dot photodynamics by polarization-rotating modulation microscopy

Toshiro Tani[a] *, Hiroshi Sakai[b], Eiji Usukura[b], Tetsu Suzuki[b] and Masaru Oda[a]

[a] *Institute of Symbiotic Science and Technology,*
[b] *Department of Applied Physics, Graduate School of Engineering,*
Tokyo University of Agriculture and Technology, Naka-cho 2-24-16, Kogane-i, Tokyo 184-8588, Japan

Received 22 June 2009; accepted 4 December 2009

Abstract

We present our recent study of polarization modulating fluorescence imaging microscopy on single CdSe colloidal quantum dots (QDs) and quantum rods (QRs) adsorbed on silica glass substrates at room temperatures. Simple optical setup is introduced to provide detection of emission profiles projected on to the sample plane as well as detection of rotating excitation polarization effect. While most studies so far in structural changes in biological or amorphous systems rely on extrinsic fluorophores with linear transition dipoles, those with twofold degenerate dipoles are noteworthy due to the intrinsic advantage for 3D orientation information. Performance of modulations is also evaluated in combination with tetramethylrodamine moieties as typical linear emitters. CdSe QDs with aspect ratio of 1.3 actually reveal plane-polarized emission at room temperature and, based on maximum-likelihood analysis, are exceptionally highly oriented on silica glass substrates.

Keywords: Single molecule detection, Imaging microscopiy, Polarization modulation, CdSe, Colloidal quantum dots, 2D transition dipole

1. Introduction

Among the various types of semiconductor quantum dots (QDs), CdSe/ZnS/Trioctylphosphineoxide (TOPO) colloidal nanocrystals are attracting much interest. Due to their core-shell structure and coordinating organic surfactants [1], they have not only high quantum yield and high optical stability but also have the advantage of having high biochemical affinity. Photoluminescence yields can be as high as 80% in toluene solution at room temperatures. CdSe/ZnS/TOPO QDs offer promise for a new type of labeling agent in protein molecules [2], DNA molecules, nuclei and cells [3]. We also have started to synthesize novel complex between CdSe QD and protein

* Corresponding author. Tel.: +81-42-388-7153; fax: +81-42-385-6255.
E-mail address: ttani@cc.tuat.ac.jp.

doi:10.1016/j.phpro.2010.01.228

molecule, molecular chaperons, in their bioactive states and been investigating photophysical dynamics to get novel insight into protein-nonprotein interactions [4].

As for the comprehension of fundamental functions of molecular chaperons such as refolding and transfer of other denatured proteins, direct trace of single-QD orientations involved in the complex must be informative. It would be useful if combined with other types of measurement such as fluorescence resonance energy transfer (FRET), where Förster-type energy transfer is expected between QD donors and Cy5 acceptors labeled on the proteins [5]. In these circumstances, we need to ascertain whether our CdSe QDs with aspect ratio of 1.3 are 2D emitters or not at room temperatures and how they are orientated on the glass substrate surface in buffer solution environment as well as in air.

While various single molecule methods, such as fluorescence-intensity trajectories [6], FRETs [7-9] and polarization methods [9-13], are capable of tracking molecular motions in real time. The last one seems to be a most sensitive tool to extract information for individual molecular orientations [14-16] and, furthermore, can be the most powerful if combined with 2D emitters. Proposal of our simple modulation optics and preliminary results on single CdSe QDs and QRs adsorbed on silica glass substrates at room temperature are described below, with data analysis and simulations.

2. Experimental

Monodispersive CdSe/ZnS/TOPO-HDA nanocrystals (QDs) (TOPO mixed with 30% of hexadecylamine) are grown in hot coordinating solvents by precisely tuned pyrolysis of organometallic compounds [17]. Average QD core diameters used for the present work are two kinds, i.e. 1.9 and 3.3 (± 0.3) nm (aspect ratio: both ca. 1.3), and ZnS shell thickness is ca. 1.7 monolayers. Size, shape and crystal phase (wurzeite structure) homogeneity are basically confirmed by high resolution TEM observations. Photoluminescence quantum yields are ca. 0.24 in average. CdSe QR nanocrystals are also synthesized with similar colloidal method in molten TOPO-Tetradecylphosphonicacid (TDPA) mixed solvent. The CdSe QRs are used without shell overcoating in the present experiments. The TEM observation confirms their rodlike shapes with diameters of 4 ~ 5 nm and lengths of 20 ~ 25 nm (aspect ratio: ca. 5). Qualities of CdSe QDs and QRs nanocrystals are also monitored by conventional UV-VIS absorption and emission spectra. Quantum yields of photoemissions are evaluated by a comparative method with rhodamine B and 6G as standards; Concentrations, temperatures, solvents, their degassing and other related protocols are precisely controlled.

As a typical linear emitter, we have used for reference florescence the labeling reagent tetramethylrhodamine (TMR) chromophores linked covalently on the surface of silica glass substrates with short alkyl chains (γ-amino proyltriethoxysilane). The former is a mixture of two isomers, 9-[2-carboxy-4(or 5)-[[(2, 5-dioxo-1-pyrrolidiyl) oxy] carbonyl] phenyl]-3,6-bis(dimethyl-amino)-xanthylium, inner salt (Molecular Probes) and used as purchased. Concentration ratio of 5- and 6- isomer is 4 : 1. Detailed procedure of the synthesis described in ref. [18].

To monitor orientation dynamics in real time, we have prepared a simple optical setup schematically illustrated in Fig. 1. Based on ordinary inverted-type optical microscope (Nikon, TE2000) with NA = 1.45 or 0.95 objective (× 100) and highly sensitive 2D-CCD (RS, Cascade-512B) detector, the rotating polarizer is introduced for excitation polarization modulation to form Köhler-type epi-illumination optics. In the situation that the relative orientation between the absorption and emission transition diploes is definitively known, and multiple observations of individual molecules can conveniently be realized by the apparatus of this type.

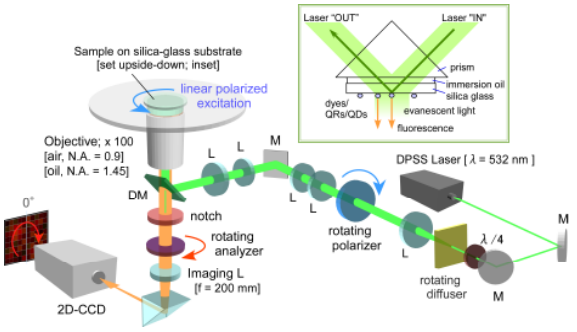

Fig. 1. Schematic set-up of polarization modulation microscope; for rotating plane polarized excitation, rotating polarizer is provided in Köhler-type epi-illumination optics and, for analyzing the emission polarization from emitters, rotating analyzer is provided within the so-called infinity space. Inset shows evanescent light illumination configuration which is used for the rotating analyzer operations. (see in the text)

One thing to be careful of is interference effects associated with the high spatial coherence of laser light source. In our system rotating diffuser is provided for homogenization and rotated as high as 2000 rpm.

In case the relation between absorption and emission dipoles being not definitive or unknown, it is much less ambiguous to analyze directly the polarization profiles of individual molecular emissions projected on to the sample plane. Thus rotating analyzer optics is fabricated and inserted in so-called infinity space. While higher quality of optical components and more precise assembly are inevitable, multiple individual detections are again realized. This point is paramount for most of the single molecule experiments. For simplicity, while in the operation of rotating polarizer, the analyzer optics is removed. In the other case of analyzer operation the polarizer rotating optics is removed and, instead, evanescent light illumination (Fig.1, inset) is used for the present works.

Single molecule observations are performed in air using NA = 0.95 objective and in HK buffer solutions by a oil-immersion NA = 1.45 objective at room temperatures. Detailed description of sample preparations for the latter is given in ref. [5].

3. Results and discussion

Lowest energy electronic excited state of CdSe nanocrystal arises when an electron is excites from an occupied Se 4p atomic orbital to empty Cd 5s orbital. This excitation is delocalized over many unit cells, and there appears pronounced dependence of the optical gap, on the size and shape of the nanocrystals. As p orbitals are 3-fold degenerate, the interaction of the Se 4p orbitals with the crystal field and the effect of spin-orbit coupling gives rise to most of the complexities in the electronic structure of CdSe nanocrystals.

The electronic structure of CdSe nanocrystals, including these complexities, has been understood theoretically based on effective mass approximations [19-21] and, more recently, with empirical pseudopotential methods [22]. Pioneering work of Sepiol et al. [23] has revealed that CdSe QDs possess 2D transition dipoles at cryogenic temperatures and this has been also confirmed at room temperatures by Chung et al. [24]. Transition from plane-polarized emission to linearly polarized one, when the nanocrystals change its shape from spherical to rodlike, is also predicted theoretically [22] and actually observed at aspect ratio of 1.25 in 3.0 nm diameter nanocrystals [25]. While there are still not realistic for the electronic predictions of each QDs with specific size and shape, here we assume 1D and 2D emission dipoles and their detection schemes are as shown in Figs. 2(a) and 2(b) for simlicity. Figure 2(c) provides typical time-trace pattern to be expected in polarization modulations and defines some parameters used in the following.

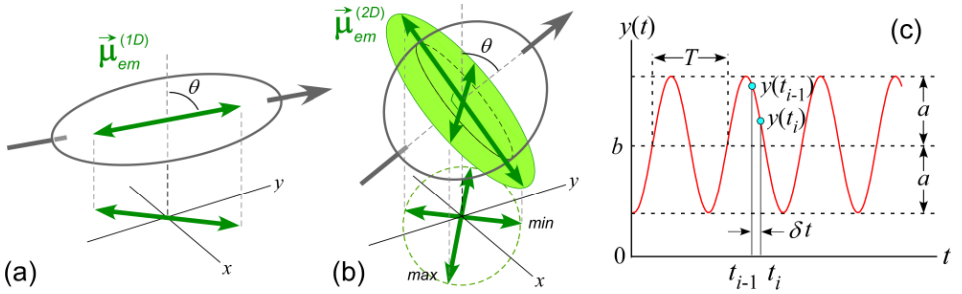

Fig. 2. Conceptual detection schemes for (a) linearly-polarized emission by a linear emitting transition dipole and (b) plane-polarized emission from a twofold degenerate dipole. Sample *xy*-plane is indicated. The graph in (c) indicates the time-trace pattern expected to be obtained by polarization modulations and the figure includes some of the parameters used in the following analysis..

Typical examples of time evolution profiles of the spot intensities from linear emitters in rotating polarizer regime are shown in Fig. 3; (a) for single TAMRA moiety and (b) and (c) for two single QRs, respectively. (b) and (c) are obtained within the same sample in simultaneous imaging. As can be seen in the figures, polarization modulations in rotating polarizer regime work well. Modulation depth M of each trajectories, defining as $M = a/b$ in Fig. 2(c), is actually equal to unity within our noise levels. This is a peculiar feature for linear emitters. Sinusoidal curves in each figure are fits to the data by $2a\cos^2(\omega t+\phi')$, where ω is an angular frequency of polarizer rotations and ϕ' is its initial phase.

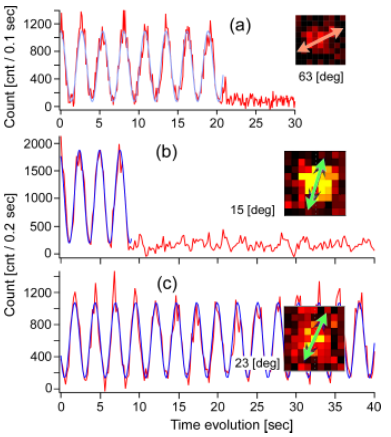

Fig. 3. Typical time evolution profiles of single linear emitters in air obtained under rotating polarizer configurations (ca. 12 rpm). The thin (red) lines correspond to the data, while thick (blue) smooth ones are simple fittings to the data by $2a\cos^2(\omega t+\phi')$. Each inset shows the respective spot image on the CCD, where arrow indicates orientation of respective dipole projection with its initial phase $\phi = 2\phi'$. (a); results on single TAMRA moiety, which ceased to emit photons at ca. 21 sec, probably due to photodegradation. 300 images are sequentially acquired with 100 msec exposure time for each and estimated excitation intensity is 122 W/cm^2. (b) and (c); those on CdSe QRs; the former shows "on" to "off" transition at ca. 8 sec, while the latter stays in its "on" state during the observation. Successive 200 images with 200 msec exposure time for each are obtained under irradiation intensity of 127 W/cm^2.

It should be noted here that, while for the moment we have obtained 17 sample spots which can be confirmed as signals from single QRs, no intermittent phase jumps has been observed. Such sudden phase jumps are often observed in case of the TAMRA moieties [18]. This is probably because QRs are rather strongly adsorbed on the glass substrates. Next, single QR are rather difficult to detect due to their lower emission yields (2.1 % in average, while (b) and (c) are the two brightest ones with probably one order of magnitude higher) and because the QRs aggregate easily. Even if these disadvatages exist, however, we conclude here the QRs with mentioned size and shape are linear emitters with their transition moment basically parallel to the directions of the long axes of the rodlike nanocrystals.

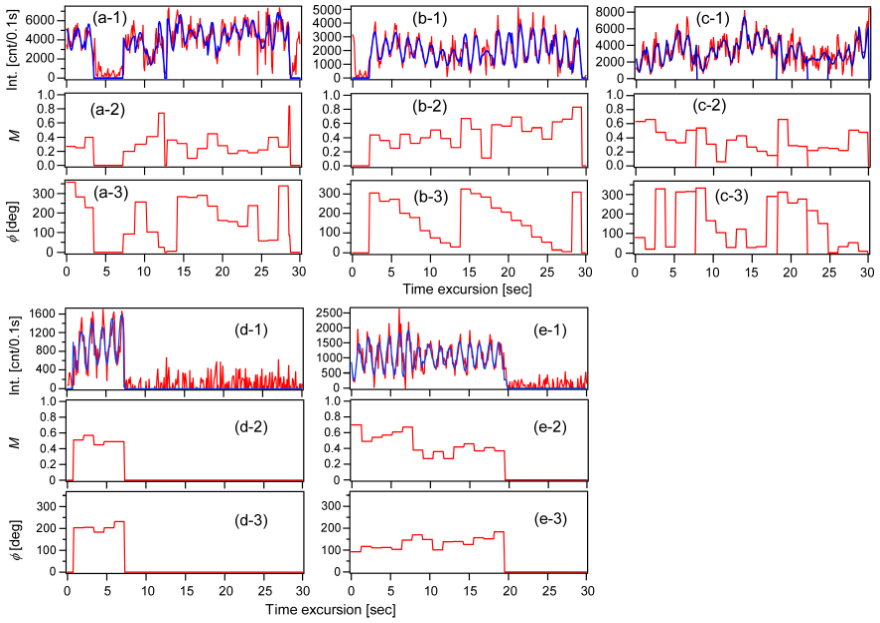

Fig. 4. Typical time evolutions of five single QDs; (a, b, c) in air and (d, e) in buffer solutions. All are adsorbed on the surface of silica glass substrates and are detected using rotating analyzer configuration with evanescent light excitation of e.g. 23.4 W/cm^2. A set of graphs labeled with (∗-1) shows experimentally obtained time excursion data and its MLE fitting for each single QDs. The thin (red) lines correspond to the former and thick (blue) smooth ones to the fittings. Those with (∗-2) and (∗-3) are the time evolution profiles of the modulation depth M and phase offset ϕ deduced from each fitting. As for the MLE analysis, see details in the text.

As for the single QDs, we have also obtained time-excursion trajectories in rotating polarizer regime and found that distinctly different characteristics from those in linear emitters mentioned above. Appearance of clear distribution in parameter M towards less than unity and sudden phase jumps accompanied with simultaneous changes in amplitude $2a$ and b parameters (Fig. 2(c)) are both definitive indications for being 2D emitters. However, instead of going into further details on the QDs, in the present paper we would rather concentrate on the results with the rotating analyzer.

In Fig.4, time-excursion profiles of emission intensities from five single CdSe QDs observed in rotating analyzer regime are displayed. These are typical and complementary examples. Those in Figs. 4(a-1) ~ 4(c-1) are obtained in air while those in Figs. 4(d-1) and 4(e-1) are in HK buffer solution. As can be seen, in air the responses are to some extent noisier and more fluctuating than those in buffer solution and, also show intermittencies and degradations. A notable feature observed in both environments is that there appears distinctly weaker modulations of $M < 1$. Clearly, these profiles are hard to the fit using the simple sinusoidal expressions given above.

To identify the nature of transition dipoles for each CdSe QDs, it is necessary to determine the time evolution of the modulation depth and direction of the projected dipoles on the sample plane (phase offset angle ϕ) for each QDs. In case of a two-fold degenerate dipole, the polar angle θ of its orientation can be determined from the modulation depth M by the relation $\cos^2\theta = (1-M) / (1+M)$ (see Fig. 2(b)). Once M and ϕ are determined for each QDs as a function of time, we can consider dynamics of the dots in 3D. To deduce M and ϕ from the data is a typical inverse problem and, for the analysis of single molecule optical measurements, several methods have already been proposed [25, 26]. Among them, we have adopted a maximum-likelihood estimator (MLE) approach proposed by Osborn et al. [26] as is certainly suitable for the present work. The Ms and ϕs indicated in Figs. 4(∗-2) and 4(∗-3) are the results of this analysis.

Before going into the results, procedure of the analysis is described briefly. We use $y(t) = b[M\cos(\omega t+\phi) + 1]$ as a fitting function and maximize a likelihood function L as given in ref. [26]; L is the probability of total N signal counts being distributed among k channels (in case of present analysis, $k = 13 \sim 15$) with n_i counts in each channel i ($i = 1$ to k). p_i is the normalized probability of finding a count in channel i. The n_i and p_i are defined as follows;

$$n_i = \int_{t_{i-1}}^{t_i} y(t)\,dt\,, \tag{1}$$

$$p_i = \frac{M}{2\pi}\left[\sin(\omega t_{i-1}+\phi) - \sin(\omega t_i+\phi)\right] + \frac{\delta t}{T}\,, \tag{2}$$

where $T = 2\pi/\omega$ is a period of modulation and δt is a length of each time bin. The best fit to the data is given by the value of M and ϕ that maximize the function L in each period. Sequential determinations by periods eventually give rise to the parameter trajectories. Computer programs are developed as macro functions on Igor Pro® ver. 6.03.

The results of the analysis are indicated in Figs. 4(∗-2) and 4(∗-3) and the best fit profiles are also shown in Figs. 4(∗-1) by thick (blue) solid lines. Accepting that the data is limited, there are some features that are notable. The characteristic to the motion of the QDs adsorbed on the substrate can be clearly seen in the figures and it can also be seen that there are some difference between the air and buffer environments. In the present paper we restrict our discussion to that relating to the modulation depth and the other aspects will be given elsewhere.

The modulation depth from the periods indicated in Figs. 4(∗-2), when combined with the values from all the periods of modulations from the trajectories of 7 QDs in air and 22 QDs in buffer, gives the histograms in Figs. 5(a) and 5(b), respectively. They can be confirmed as being single QDs from those obtained simultaneously within the identical imaging, and also weight corrections due to the on-state time differences in each QDs are included. While for the moment accumulated numbers of the data available are limited, we can see there appears broad but distinctive peak in each histogram. Most of the M events distribute in less than unity indicates that the QDs observed are not only 2D emissions in nature but also they are unexpectedly oriented on the surface of substrate. In case of isotropic distribution in orientation of 2D emitters, we can estimate the distribution profile analytically; the result of which is given by $D(M) \propto (1+M)^{-3/2}(1-M)^{-1/2}$ and is also indicated by the solid line in Fig. 5(a). The singularity appeared at $M \to 1$ is a van-Hove-type singularity in one-dimensional systems. We can see distinctive convergence in the orientations of the QDs is apparent.

In order to see how the orientations of the QDs are distributed, we have also performed simple numerical simulations assuming Gaussian distribution of 2D transition dipoles around one specific orientation. Parameters to

be simulated are again seen in Fig. 2(b), where polar angle θ should be Gaussian while longitudinal angle, equals to the phase offset ϕ introduced above, is assumed to be isotropic. Numerical protocols are also prepared on the macro functions in the Igor Pro. The simulated distributions obtained are also shown in Figs. 5(a) and 5(b) by the curves made of + marks, respectively, and the observed features are reproduced sufficiently for the moment. Estimated orientation peak angles as well as its standard deviations (θ_0, δ_0) are (43°, 35°) in air (a) and (55°, 33°) in buffer (b), respectively. Existence of exceptionally highly oriented distributions is concluded for the CdSe QDs with average diameters of 1.9 and 3.3 nm (aspect ratio: ca. 1.3). They are not in perpendicular (θ_0 = 0°) to the sample plane nor horizontal (θ_0 = 90°). As for the difference seen in the different environments of air and buffer solution, though the detailed observed properties seem to be discriminating to some extent, we think it is not decisive yet. It is also not clear for the moment why such narrow distributions are realized. Some kinds of peculiarities in the shape or organic ligands of the QDs can affect the adsorption processes resulting in the anisotropic conformation on the silica glass surface.

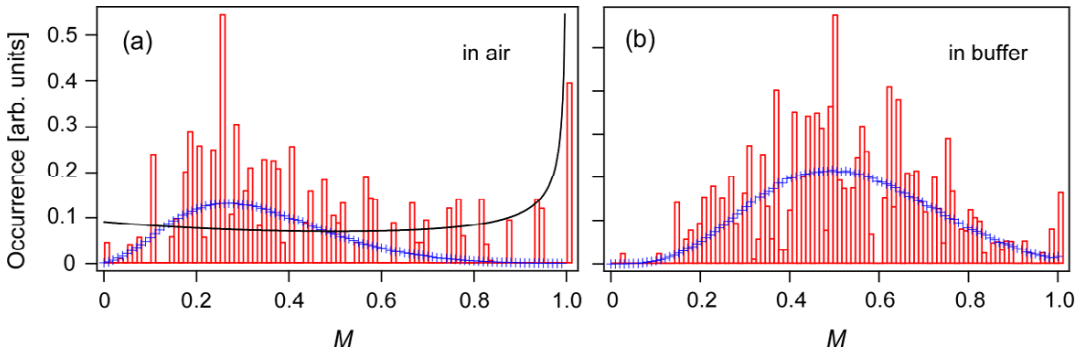

Fig. 5. Modulation-depth histograms of QDs in air (a) and in buffer solutions (b); both of which are composed from the results of analysis presented in Fig.4. Profiles formed with rather small + marks in each figures indicate the results of simulation assuming the distribution of the dipole orientations is Gaussian. Simulations provide a peak and a standard deviation for each distribution; they are (a) $\theta_0 = 43°$, $\delta_0 = 35°$ in air and (b) $\theta_0 = 55°$, $\delta_0 = 33°$ in buffer solution, respectively. In (a), predicted distribution profile (solid line) for random isotropic dipole orientations is also shown for reference.

It should be noted lastly that the histograms presented in Figs. 5 neglect the aspects of time evolution properties totally. The data and parameters in Figs. 4 indicate the existence of some continuously fluctuating natures during on-states in addition to the sudden intermittent jumps. Phase offset ϕ also shows drifting or to some extent rotating tendencies in air while it is rather stable in buffer. In the previous work on the blinking mechanism of the QDs, we have proposed the existence of surface trap-state, and its charge can be modified extrinsically by the adsorptions of pole species such as H_2O molecules [27]. This means that the transition dipoles of the QDs while in on-states can be fluctuated from time to time if the adsorbed state is fluctuating. If more than one traps may exist on each single QDs, the effect will be larger. Thus even a possibility of separated motion of the transition dipole from the real motion of the QD should not be neglected. This would be quite a new optoelectronic feature of QDs and should further be elucidated. Systematic and more sophisticated investigations are now underway, both in shape and size control of QDs as well as in optimization of experimental conditions and analysis for the polarization modulation.

In conclusion, we have developed a simple and versatile polarization modulation microscope and demonstrated its performance using CdSe colloidal QRs and QDs as 1D and 2D transition dipole emitters. We have found the QDs are exceptionally highly oriented on adsorbed silica glass substrates both in air and in buffer even at room temperature. This is surely an encouraging feature if for instance the QDs are to have applications in quantum-photonics such as in nanoscale arrays in the near future.

Acknowledgements

This work is partly supported by grants-in-aid from Ministry of Education, Science, Sports and Culture, No. 21651066, and New Energy and Industrial Technology Development Organization (NEDO), No. 08C46615c.

References

[1] B. O. Dabbousi, J. Rodriguez-Viejo, F. V. Mikulec, J. R. Heine, H. Mattoussi, R. Ober, K. F. Jensen, M. G. Bawendi, *J. Phys. Chem. B*, **101** (1997) 9463.
[2] W. C. W. Chan, S. Nie, *Science,* **281** (1988) 2016.
[3] A. R. Clapp, I. L. Medintz, J. Mattew Maruro, B. R. Fisher, M. G. Bawendi, H. Mattoussi, *J. Am. Chem. Soc.*, **126** (2004) 301.
[4] H. Horiuchi, E. Usukura, A. Ohtaki, T. Zako, M. Oda, M. Yohda, T. Tani, *J. Lumin*. **127** (2007) 192.
[5] T. Tani, H. Horiuchi, M. Oda, E. Usukura, H. Sakai, A. Ohtaki, M. Yohda, *Phys. Statas Solidi*, **C6** (2009) 912.
[6] H. P. Lu, L. Xun, X. S. Xie, *Science*, **282** (1998) 1877.
[7] X. Zhuang, T. Ha, H. Babcock, H. Kim, S. Chu, L. Bartley, R. Russell, D. Herschlag, *Front. Sci. Ser.*, **31** (2000) 29.
[8] T. Ha, *Single Mol.*, **2** (2001) 283.
[9] S. Weiss, *Nat. Struct. Biol.*, **7** (2000) 724.
[10] J. F. Forkey, M. E. Quinlan, Y. E. Goldman, Prog. Biophys. *Mol. Biol.*, **74** (2000) 1.
[11] T. Ha, A. Y. Ting, J. Liang, W. B. Caldwell, A. A. Deniz, D. S. Chemla, P. G. Schultz, S. Wess, *Proc. Natl. Acad. Sci. USA*, **96** (1999) 893.
[12] D. M. Warshaw, E. Hayes, D. Gaffney, A.-M. Lauzon, J. Wu, G. Kennedy, K. Trybus, S. Lowey, C. Berger, *Proc. Natl. Acad. Sci. USA*, **95** (1998) 8034.
[13] K. D. Weston, L. S. Goldner, *J. Phys. Chem. B*, **105** (2001) 3453.
[14] T. Ha, T. Enderle, D. S. Chemla, P. R. Selvin, S. Weiss, *Phys. Rev. Lett.*, **77** (1996) 3979.
[15] T. Ha, J. Glass, T. Enderle, D. S. Chemla, S. Weiss, *Phys. Rev. Lett.*, **80** (1998) 2093.
[16] T. Ha, T. A. Laurence, D. S. Chemla, S. Weiss, *J. Phys. Chem. B*, **103** (1999) 6839.
[17] M. Oda, J. Tsukamoto, A. Hasegawa, N. Iwami, K. Nishiura, I. Hagiwara, N. Ando, H. Horiuchi, T. Tani, *J. Lumin.*, **122-123** (2007) 762; K. Hashizume, M. Matsubayashi, M. Vacha, T. Tani, *J. Lumin.*, **98** (2002) 49.
[18] T. Tani, K. Mashimo, T. Suzuki, H. Horiuchi, M. Oda, *J. Lumin.*, **128** (2008) 757.
[19] Al. L. Efros, *Phys. Rev. B*, **46** (1992) 7448.
[20] Al. L. Efros and M. Rosen, M. Kuno, M. Nirmal, D. J. Norris, and M. Bawendi, *Phys. Rev. B*, **54** (1996) 4843.
[21] Al. L. Efros and M. Rosen, *Annu. Rev. Mater. Sci.*, **30** (2000) 475.
[22] L-W. Wang, A. Zunger, *Phys. Rev. B*, **53** (1996) 9579.
[23] J. Sepiol, J. Jasny, J. Keller, U. P. Wild, *Chem. Phys. Lett.*, **273** (1997) 444.
[24] I. Chung, K. T. Shimizu, M. G. Bawendi, *Proc. Natl. Acad. Sci. USA*, **100** (2003) 405.
[25] e.g. T. Mutoh, lecture note on maximum entropy method (in Japanese, 1997; private communication), L. P. Watkins, H. Yang, *J. Phys. Chem. B*, **109** (2005) 617, *ibid*, *Biophys. J.*, **86** (2004) 4015, and references therein.
[26] K. D. Osborn, M. K. Singh, R. J. Bieber Urbauer, C. K. Johnson, *CHEMPHYSCHEM*, **4** (2003) 1005.
[27] M. Oda, A. Hasegawa, N. Iwami, K. Nishiura, N. Ando, A. Nishiyama, H. Horiuchi, T. Tani, *J. Lumin.*, **127** (2007) 198.